The Astrophysical Journal, 729:15 (12pp), 2011 March 1 doi:10.1088/0004-637X/729/1/15

ON THE *ORTHO*:*PARA* RATIO OF H_3^+ IN DIFFUSE MOLECULAR CLOUDS*

Kyle N. Crabtree[1], Nick Indriolo[2], Holger Kreckel[1], Brian A. Tom[1,4], and Benjamin J. McCall[1,2,3]
[1] Department of Chemistry, University of Illinois at Urbana-Champaign, Urbana, IL 61801, USA
[2] Department of Astronomy, University of Illinois at Urbana-Champaign, Urbana, IL 61801, USA
[3] Department of Physics, University of Illinois at Urbana-Champaign, Urbana, IL 61801, USA
Received 2010 August 31; accepted 2010 December 23; published 2011 February 4

ABSTRACT

The excitation temperature T_{01} derived from the relative intensities of the $J = 0$ (*para*) and $J = 1$ (*ortho*) rotational levels of H_2 has been assumed to be an accurate measure of the kinetic temperature in interstellar environments. In diffuse molecular clouds, the average value of T_{01} is ∼70 K. However, the excitation temperature $T(H_3^+)$ derived from the $(J, K) = (1, 1)$ (*para*) and $(1, 0)$ (*ortho*) rotational levels of H_3^+ has been observed to be ∼30 K in the same types of environments. In this work, we present observations of H_3^+ in three additional diffuse cloud sight lines for which H_2 measurements are available, showing that in four of five cases T_{01} and $T(H_3^+)$ are discrepant. We then examine the thermalization mechanisms for the *ortho*:*para* ratios of H_3^+ and H_2, concluding that indeed T_{01} is an accurate measure of the cloud kinetic temperature, while the *ortho*:*para* ratio of H_3^+ need not be thermal. By constructing a steady-state chemical model taking into account the nuclear spin dependence of reactions involving H_3^+, we show that the *ortho*:*para* ratio of H_3^+ in diffuse molecular clouds is likely governed by a competition between dissociative recombination with electrons and thermalization via reactive collisions with H_2.

Key words: astrochemistry – ISM: molecules – molecular processes

Online-only material: color figures

1. INTRODUCTION

Observations of H_3^+ in diffuse molecular clouds (diffuse clouds in which a significant fraction of the hydrogen is in molecular form; Snow & McCall 2006) have led to various unexpected discoveries. The very first detection of H_3^+ along a diffuse molecular cloud sight line (toward Cyg OB2 12) showed an abundance about 10 times greater than expected for the environment (McCall et al. 1998a). This surprising overabundance—also found toward several more diffuse cloud sight lines—led to the eventual conclusion that the ionization rate of H_2 due to cosmic rays, ζ_2, must be about one order of magnitude larger than previously thought (McCall et al. 2003; Indriolo et al. 2007). Another puzzling outcome from H_3^+ observations is that the average excitation temperature derived from the two lowest energy states ($\langle T(H_3^+)\rangle \approx 30$ K; Indriolo et al. 2007) differs significantly from the average excitation temperature derived from the two lowest rotational states of H_2 ($\langle T_{01}\rangle \approx 70$ K; Savage et al. 1977; Rachford et al. 2002, 2009). Given that both species are expected to be thermalized to the cloud kinetic temperature by collisions, such a discrepancy is unexpected.

Despite the fact that the $J = 0$ and $J = 1$ levels of H_2 are essentially different "species"—conversion between the even-J *para* and odd-J *ortho* nuclear spin states is only possible through reactive collisions—it has long been assumed that T_{01} is a good approximation for the kinetic temperature, $T_{\rm kin}$, in diffuse molecular clouds. This is because H_2 molecules are expected to experience many reactive collisions with protons during their lifetimes. As a result, the *ortho* and *para* populations of H_2 should be brought into thermal equilibrium with the proton kinetic temperature (Dalgarno et al. 1973).

Similarly, H_3^+ also has *ortho* and *para* nuclear spin states ($(J, K) = (1, 1)$ is the lowest lying *para* state, and $(J, K) = (1, 0)$ the lowest lying *ortho* state). For H_3^+ though, the relative population between the two states has been expected to be thermalized by reactive collisions with H_2 (McCall et al. 1998b, 2003; Gibb et al. 2010). As the average values of T_{01} and $T(H_3^+)$ do not agree, this does not seem to be the case.

However, out of the 66 and 18 sight lines used to compute $\langle T_{01}\rangle$ and $\langle T(H_3^+)\rangle$, respectively, only two are shared between both samples. While previously reported values of T_{01} and $T(H_3^+)$ do differ for these sight lines toward ζ Per and X Per by about 30 K (Savage et al. 1977; Rachford et al. 2002; Indriolo et al. 2007), such a small sample does not provide particularly meaningful results. In order to increase the number of sight lines with *ortho* and *para* column densities determined for both H_2 and H_3^+, we have made observations searching for H_3^+ absorption features along sight lines with measured H_2 column densities. These observations and our data reduction procedures are described in Section 2. Section 3 discusses and justifies many of the assumptions made concerning molecular hydrogen and T_{01} in diffuse molecular clouds. In Section 4, we examine the $H_3^+ + H_2$ reaction and present steady-state models to explore the temperature discrepancy between T_{01} and $T(H_3^+)$. Section 5 reviews the observations and modeling, and presents our conclusions from the work.

2. OBSERVATIONS AND DATA REDUCTION

Target sight lines were selected based on H_2 column densities (Savage et al. 1977; Rachford et al. 2002, 2009) and L-band magnitudes. We required that the $J = 0$ and $J = 1$ column densities of H_2 ($N(0)$ and $N(1)$, respectively) both be known, and that the total H_2 column density ($N(H_2)$) be greater than 10^{20} cm^{-2}. The L-band magnitude was required to be brighter than 6 mag so that the necessary integration times would be relatively short.

* Based in part on observations made with ESO Telescopes at the La Silla or Paranal Observatories under program ID 384.C-0618.
[4] Current address: Department of Chemistry, United States Air Force Academy, CO 80840, USA.

Table 1
Observations

Object	Date(s) of Observation	Telescope	Integration Time (minutes)	Standard
HD 149404	2009 Aug 5	Gemini South	32	λ Sco
χ Oph	2009 Aug 30	Gemini South	12	λ Sco
HD 152236	2009 Aug 30	Gemini South	16	λ Sco
HD 154368	2009 Aug 30	Gemini South	32	λ Sco
HD 53367	2009 Dec 3	VLT	30	κ Ori
HD 73882	2009 Dec 3	VLT	30	ζ Pup
	2010 Jan 17	VLT	30	ζ Pup
HD 110432	2010 Jan 27	VLT	10	η Cen
	2010 Feb 28	VLT	20	η Cen
	2010 Mar 2	VLT	40	η Cen
μ Nor	2010 Apr 5	Gemini South	72	λ Sco

Observations focused on the $R(1, 1)^u$, $R(1, 0)$, and $R(1, 1)^l$ transitions (at 3.668083 μm, 3.668516 μm, and 3.715479 μm, respectively) which arise from the $(J, K) = (1, 1)$ and $(1, 0)$ levels of the ground vibrational state of H_3^+, the only levels expected to be significantly populated at average diffuse cloud temperatures ($T \sim 70$ K).

Spectra in support of this project were obtained using the Phoenix spectrometer (Hinkle et al. 2003) at the Gemini South Telescope and the Cryogenic High-resolution Infrared Echelle Spectrograph (CRIRES; Käufl et al. 2004) at the Very Large Telescope (VLT). Observations at Gemini South were made in queue mode, and the Phoenix spectrometer was used with its echelle grating and 0.″17 slit to produce a resolving power of about 70,000, and with the L2734 filter to select the order containing the $R(1, 1)^u$ and $R(1, 0)$ transitions. Observations at the VLT were made in service mode, and CRIRES was used with its 0.″2 slit to provide a resolving power of about 100,000, and a reference wavelength of 3715.0 nm to cover the $R(1, 1)^u$ and $R(1, 0)$ transitions on detector 1 and the $R(1, 1)^l$ transition on detector 3. The adaptive optics system was used with CRIRES to maximize starlight passing through the narrow slit. In addition to the science targets, bright, early-type stars were observed for use as telluric standards. For all observations, the star was nodded along the slit in an ABBA pattern in order to facilitate the removal of atmospheric emission lines and dark current via the subtraction of neighboring images. A log containing the observed sight lines and respective integration times is given in Table 1.

Various standard IRAF[5] procedures were used in the data reduction process. Given the different state of data available from Phoenix versus CRIRES, different amounts of processing were required for data from the two telescopes. For each night of Phoenix observations, a bad pixel map was created from the average of several dark frames, and these pixels were interpolated over in the object and flat frames. Flats were then combined to create a normalized flat field which was divided out of the object frames. Neighboring AB image pairs were subtracted from each other to remove atmospheric emission and dark current. Finally, one-dimensional spectra were extracted using *apall*. In the case of CRIRES observations, data were processed through the CRIRES specific pipeline, resulting in fully reduced two-dimensional spectral images for each target (given the product codes SCOM and PCOM by the pipeline). One-dimensional spectra were extracted from these images. All

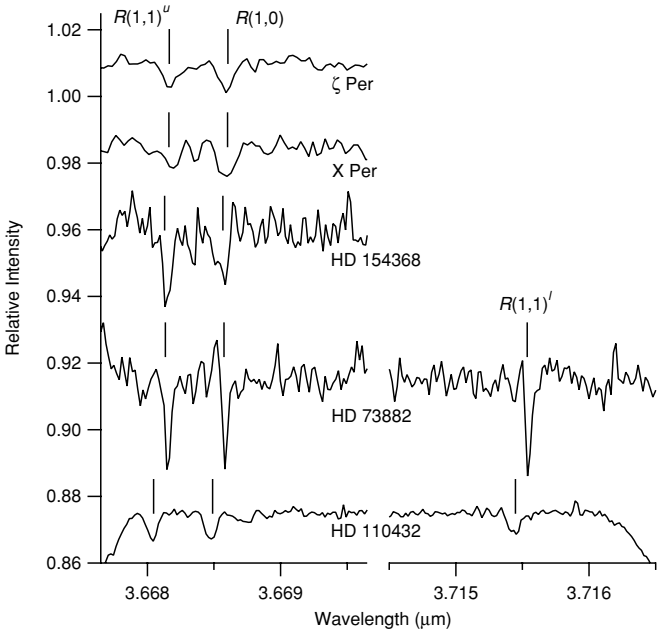

Figure 1. Spectra showing absorption lines from the $(J, K) = (1, 1)$ and $(1, 0)$ states of H_3^+. Spectra for ζ Per and X Per were taken at UKIRT and are reprocessed versions of the data previously reported in Indriolo et al. (2007). The spectrum for HD 154368 was taken at Gemini South, while those for HD 73882 and HD 110432 were taken at the VLT. Large deviations from flat continuum levels in the spectra for HD 154368, HD 73882, and HD 110432 are the combination of two effects: (1) artifacts due to continuum fitting at wavelengths far away from the H_3^+ absorption lines and (2) inability to remove the strong atmospheric methane line immediately shortward of the $R(1, 1)^u$ line. Vertical lines mark the expected positions of the H_3^+ absorption lines given previously determined interstellar gas velocities along each sight line.

such spectra from both telescopes were then imported to IGOR Pro[6] where the remainder of reduction was performed.

Individual Phoenix spectra within an exposure sequence for a given target were then added together. Science target spectra from both telescopes were divided by telluric standard spectra to remove atmospheric absorption features and to normalize each spectrum. These normalized spectra were wavelength calibrated with a typical accuracy of ∼2 km s^{-1} using the vacuum wavelengths of the atmospheric absorption lines. Calibrated spectra were then shifted into the local standard of rest (LSR) frame, and spectra of the same target from different nights were combined using a variance-weighted mean. For each sight line, the continuum surrounding the absorption features was then fit with an nth-order polynomial ($n = 7$–9) and the spectrum was divided by the fit to re-normalize the continuum level. The resulting spectra for sight lines with H_3^+ absorption features—HD 154368, HD 73882, and HD 110432—are shown in Figure 1. Although H_3^+ spectra for ζ Per and X Per (the other two sight lines with both H_2 and H_3^+ data) are reported in Indriolo et al. (2007), the reduction process utilized in that study did not combine spectra using a variance-weighted mean, nor did it fit fluctuations in the continuum level with a polynomial function. For the purpose of consistency, we have reprocessed the data from both sight lines. No new data have been added, but differences in the method of processing have resulted in output spectra with slightly better signal-to-noise ratios (S/N). These spectra are also shown in Figure 1.

Absorption features due to H_3^+ were fit with Gaussian functions in order to determine equivalent widths, velocity FWHM,

[5] http://iraf.noao.edu/

[6] http://www.wavemetrics.com/

Table 2
Absorption Line Parameters

Object	Transition	v_{LSR} (km s^{-1})	FWHM (km s^{-1})	W_λ (10^{-6} μm)	$\sigma(W_\lambda)$ (10^{-6} μm)	$N(J,K)$ (10^{13} cm^{-2})	$\sigma(N)$ (10^{13} cm^{-2})
ζ Per	$R(1, 1)^u$	7.7	11.0	0.99	0.13	4.09	0.53
	$R(1, 0)$	6.1	9.0	1.00	0.11	2.53	0.29
X Per	$R(1, 1)^u$	8.2	9.1	0.80	0.17	3.34	0.69
	$R(1, 0)$	6.3	10.2	1.30	0.18	3.29	0.45
HD 154368	$R(1, 1)^u$	5.4	6.0	1.79	0.30	7.43	1.24
	$R(1, 0)$	5.2	5.6	1.12	0.29	2.83	0.74
HD 73882	$R(1, 1)^u$	5.9	3.9	1.44	0.21	5.97	0.86
	$R(1, 0)$	5.7	3.2	1.16	0.19	2.94	0.48
	$R(1, 1)^l$	5.4	3.5	1.34	0.15	6.15	0.69
HD 110432	$R(1, 1)^u$	−3.8	6.9	0.74	0.06	3.08	0.24
	$R(1, 0)$	−3.3	7.5	0.83	0.07	2.11	0.17
	$R(1, 1)^l$	−3.1	8.1	0.69	0.06	3.15	0.28

Notes. Column 3 (v_{LSR}) gives the interstellar gas velocity in the local standard of rest frame. Column 4 (FWHM) gives the full width at half-maximum of the absorption features. Columns 5 and 6 show the equivalent width, W_λ, and its 1σ uncertainty, $\sigma(W_\lambda)$, respectively. Columns 7 and 8 give the column density of H_3^+ in the state each transition probes, $N(J,K)$, and its uncertainty, $\sigma(N)$, respectively. Values for these parameters in the ζ Per and X Per sight lines were previously reported in Indriolo et al. (2007). The new values for both absorption lines toward ζ Per and the $R(1, 0)$ line toward X Per are consistent with the previously published results within uncertainties. However, the new and old results for the $R(1, 1)^u$ line toward X Per are inconsistent. Upon inspection, we found this to be due to a bad fit to that line during the 2007 analysis. In all cases, the values published herein should be taken to supersede those from Indriolo et al. (2007).

Table 3
Target Sight Line Properties

Quantity	Units	ζ Per[a,b]	X Per[a,c]	HD 154368[c]	HD 73882[c]	HD 110432[c,d]
			H_3^+ Results			
$N(1, 1)$	(10^{13} cm^{-2})	4.09 ± 0.53	3.34 ± 0.69	7.43 ± 1.24	6.08 ± 0.12	3.11 ± 0.05
$N(1, 0)$	(10^{13} cm^{-2})	2.53 ± 0.29	3.29 ± 0.45	2.83 ± 0.74	2.94 ± 0.48	2.11 ± 0.17
p_3[e]		0.62 ± 0.04	0.50 ± 0.06	0.72 ± 0.06	0.67 ± 0.04	0.60 ± 0.02
$T(H_3^+)$	(K)	28 ± 4	46^{+21}_{-13}	20 ± 4	23 ± 3	30 ± 2
			H_2 Results			
log[$N(0)$]	(cm^{-2})	20.51 ± 0.09	20.76 ± 0.03	21.04 ± 0.05	20.99 ± 0.08	20.40 ± 0.03
log[$N(1)$]	(cm^{-2})	20.18 ± 0.09	20.42 ± 0.06	20.54 ± 0.15	20.50 ± 0.07	20.27 ± 0.04
p_2[f]		0.68 ± 0.06	0.69 ± 0.04	0.76 ± 0.07	0.76 ± 0.05	0.57 ± 0.03
T_{01}	(K)	58 ± 6	57 ± 4	51 ± 8	51 ± 6	68 ± 5

Notes. Measured column densities for the lowest lying *ortho* and *para* states of H_2 and H_3^+ are shown for the five sight lines with all such data available. Also shown are the *para*-fractions for each species and the rotational temperatures derived from a simple two-state system analysis.
[a] Updated analysis of H_3^+ data originally presented in Indriolo et al. (2007).
[b] H_2 data from Savage et al. (1977).
[c] H_2 data from Rachford et al. (2002).
[d] May be affected by multiple velocity components (Crawford 1995).
[e] *p*-H_3^+ fraction: $N(1, 1)/(N(1, 0) + N(1, 1))$.
[f] *p*-H_2 fraction: $N(1)/(N(0) + N(1))$.

and interstellar gas velocities. Our fitting procedure uses the functional form of a Gaussian where the area (as opposed to amplitude) is a free parameter, and includes a fit to the continuum level, y_0. In the case of the $R(1, 1)^u$ and $R(1, 0)$ lines, both absorption features are fit simultaneously and a single best-fit continuum level is found. Uncertainties on the equivalent widths (δW_λ) and continuum level (δy)—both at the 1σ level—were output by the fitting process. To estimate the systematic uncertainties due to continuum placement, we forced the continuum level to $y_0 + \delta y$ and $y_0 - \delta y$ and re-fit the absorption lines. Variations in the equivalent widths due to this shift are small compared to those reported by the fitting procedure and so are not included in our analysis (i.e., $\sigma(W_\lambda) = \delta W_\lambda$). Assuming optically thin absorption lines and taking transition dipole moments and wavelengths from Goto et al. (2002) and references therein, column densities were derived from equivalent widths using the standard relation. All of these results are shown in Table 2.

These observations increase the total number of sight lines with both H_3^+ and H_2 detections from 2 to 5. Column densities, *para*-fractions, and excitation temperatures for both species along all five sight lines are collected in Table 3. H_2 data come from Savage et al. (1977) and Rachford et al. (2002). Uncertainties on all values are 1σ. The excitation temperatures inferred from the $R(1, 0)$, $R(1, 1)^u$, and $R(1, 1)^l$ absorption lines of H_3^+ range from $20 \leqslant T(H_3^+) \leqslant 46$ K, while those reported for H_2 vary from $51 \leqslant T(H_2) \leqslant 68$ K. In four sight lines T_{01} is greater than $T(H_3^+)$ by about 30 K, while for X Per

T_{01} and $T(H_3^+)$ are consistent within uncertainties. Still, these observations clearly show that for the same interstellar material along four different diffuse molecular cloud sight lines, the excitation temperatures derived from H_3^+ and H_2 do not agree.

3. H_2 THERMALIZATION

Given the large discrepancies between T_{01} inferred from H_2 and the excitation temperature of H_3^+, it is important to re-examine the assumption that the inferred T_{01} accurately reflects the kinetic temperature of the diffuse molecular clouds. If this assumption were incorrect, it would be conceivable that H_3^+ provides the true (lower) temperature of diffuse molecular clouds. There are at least four reasons this assumption could be invalid: (1) observational errors in the determination of the $J = 0$ and $J = 1$ column densities of H_2, (2) an insufficient frequency of $H^+ + H_2$ collisions to achieve steady state, (3) the steady state of this reaction being different from the thermodynamic equilibrium, and (4) errors caused by a varying $J = 0$:1 ratio along the line of sight. In the following subsections, we investigate each of these possibilities in turn.

3.1. Observational Determination of H_2 Columns

The measurement of the column densities of $J = 0$ and $J = 1$ of H_2 is performed by profile fitting to spectra of the Lyman (A–X) band in the ultraviolet, recorded with *Copernicus* or *Far-Ultraviolet Spectroscopic Explorer*. The H_2 transitions are optically thick, and are completely opaque in the line cores. Given the difficulties in accurately retrieving column densities from optically thick transitions, one might worry that the inferred T_{01} is contaminated by uncertainties caused by radiative transfer.

According to B. L. Rachford (2010, private communication), the detailed shape of the combined profile of the $J = 0$ line and the two $J = 1$ lines is quite sensitive to the ratio of the column densities of these two rotational levels, and thus provides a very useful probe of T_{01}. Because multiple vibronic bands of H_2, which are known to be relatively free of contamination by stellar lines, are used in the determination of T_{01}, it is difficult to envision any systematic errors that could affect the measurements. The statistical errors in the column density measurements are typically ∼0.1 dex, and we can therefore conclude that the ultraviolet measurements provide an accurate and fairly precise measure of the ratio of $N(0)$ to $N(1)$ for H_2.

3.2. Frequency of $H^+ + H_2$ Reactions

The $J = 0$ and $J = 1$ rotational levels of H_2 belong to different spin modifications (*para* and *ortho*, respectively) and are therefore not thermalized by non-reactive collisions or radiative transitions. Only chemical reactions, in which the protons are exchanged, can affect the nuclear spin modification of H_2.[7]

Since H_2 is formed in a highly exothermic reaction on grain surfaces, its nascent rotational (and spin) distribution is presumed to represent a high temperature (Takahashi 2001). In the high-temperature limit, H_2 should be formed with an *ortho*:*para* ratio of 3:1. If an insufficient number of reactive collisions occur between the formation of an H_2 molecule and its subsequent destruction (by photodissociation or cosmic-ray ionization), then the average *ortho*:*para* ratio of H_2 may lie somewhere between the nascent value (3:1) and the thermalized value (1:2 at 60 K, for example). This could lead to T_{01} overestimating the true cloud kinetic temperature.

The number of reactive collisions suffered by an average H_2 molecule in its lifetime can be expressed as $\mathcal{N}_{\rm rxn} \equiv \tau_{\rm life}/\tau_{\rm rxn}$, where $\tau_{\rm life}$ is the average lifetime of an H_2 molecule and $\tau_{\rm rxn}$ is the average time between reactive collisions. If $\mathcal{N}_{\rm rxn} \gg 1$, then the *ortho*:*para* ratio of H_2 should reflect the steady state of the reaction in question.

In diffuse molecular clouds, H_2 is formed on grains at a rate of $Rn_{\rm H}n({\rm H})$, where R is the grain formation rate (typically taken to be about 3×10^{-17} cm^3 s^{-1}, e.g., Spitzer 1978; Gry et al. 2002), $n_{\rm H} \equiv n({\rm H}) + 2n(H_2)$ is the total number density of hydrogen nuclei, and n(H) is the number density of atomic hydrogen. The destruction of H_2 is dominated by cosmic-ray ionization and photodissociation (following absorption in the Lyman bands), and has a rate of $(\zeta_2 + \Gamma)n(H_2)$, where Γ is the photodissociation rate. In steady state, these two rates are equal, and we can solve for $\tau_{\rm life} = (\zeta_2 + \Gamma)^{-1} = n(H_2)/[Rn_{\rm H}n({\rm H})]$. By using the definition of the local molecular fraction $f^n_{H_2} \equiv 2n(H_2)/n_{\rm H}$ (which we will simply call f), we can rewrite this expression as $\tau_{\rm life} = f/[2Rn_{\rm H}(1 - f)]$.

Assuming that the reaction of $H^+ + H_2$ dominates the interconversion of o-H_2 and p-H_2(*ortho*- and *para*-H_2, respectively), we can write $\tau_{\rm rxn} = [k_{\rm ic}n(H^+)]^{-1}$, where $k_{\rm ic}$ is the rate coefficient for the interconversion reaction. Substituting the expressions for $\tau_{\rm life}$ and $\tau_{\rm rxn}$ into the equation for $\mathcal{N}_{\rm rxn}$, we find

$$\mathcal{N}_{\rm rxn} = \frac{k_{\rm ic}}{R}\frac{n(H^+)}{n_{\rm H}}\frac{f}{2(1-f)}.$$

To estimate the number density of H^+, we consider the steady state of its formation and destruction. H^+ is formed by cosmic-ray ionization of H atoms, at a rate of $\zeta_{\rm H}n$(H), where $\zeta_{\rm H}$ is the cosmic-ray ionization rate of H ($2.3\zeta_{\rm H} \approx 1.5\zeta_2$; Glassgold & Langer 1974). Given the abundances of various species in diffuse clouds and the rate coefficients for reactions between H^+ and such species, chemical models (e.g., Woodall et al. 2007) predict that H^+ is destroyed predominantly by charge transfer to atomic oxygen, with a rate of $k_{\rm ct}n(H^+)n$(O). Equating these rates of formation and destruction and solving for $n(H^+)$, we find $n(H^+) = \zeta_{\rm H}(1 - f)/[k_{\rm ct}x({\rm O})]$, where $x({\rm O}) \equiv n({\rm O})/n_{\rm H}$. Finally, substituting this into the expression for $\mathcal{N}_{\rm rxn}$ gives

$$\mathcal{N}_{\rm rxn} = \frac{k_{\rm ic}}{R}\frac{\zeta_{\rm H}}{k_{\rm ct}}\frac{f}{2n_{\rm H}}\frac{1}{x({\rm O})}.$$

Adopting values of $k_{\rm ic} = 2.2 \times 10^{-10}$ cm^3 s^{-1} (Gerlich 1990), $R = 3 \times 10^{-17}$ cm^3 s^{-1}, $\zeta_2 = 4 \times 10^{-16}$ s^{-1} (Indriolo et al. 2007), $k_{\rm ct} = 7.31 \times 10^{-10}(T/300)^{0.23}e^{-225.9/T}$ cm^3 s^{-1} (Woodall et al. 2007), $x({\rm O}) \approx 3 \times 10^{-4}$ (Cartledge et al. 2004; Jensen et al. 2005), and typical diffuse cloud values of $f = 0.9$[8] and $n_{\rm H} = 100$ cm^{-3} (Snow & McCall 2006), we find that at $T \sim 70$ K, $\mathcal{N}_{\rm rxn} \sim 1400$. Thus, the typical H_2 molecule will experience over 1000 reactive collisions during its lifetime, and we can safely assume that the initial *ortho*:*para* ratio of H_2 is irrelevant; instead, the observed *ortho*:*para* ratio should reflect the steady state of the reactive collisions.

[7] Strictly speaking, large inhomogeneous magnetic fields, such as found on the surface of paramagnetic catalysts, can also affect the nuclear spin modification of H_2, but we assume that such effects are negligible in interstellar conditions.

[8] While the line-of-sight molecular fraction is lower, that quantity integrates over atomic gas not associated with the diffuse molecular cloud. We are therefore using the local molecular fraction typical of diffuse molecular clouds.

3.3. Steady State of $H^+ + H_2$ Reactions

From a thermodynamic perspective, one would expect that the steady state of the $H^+ + H_2$ reaction would represent a thermal distribution of *o*-H_2 and *p*-H_2, if no other processes influence the spin modifications. This expectation has been confirmed by a phase space theoretical calculation by Gerlich (1990), who found that the *ortho*:*para* ratio could be expressed at low temperatures (30–80 K) by the expression $9.35\exp(-169.4/T)$, quite close to the thermodynamic expectation of $9\exp(-170.4/T)$. Evidently, the nuclear spin selection rules for this chemical reaction, which suppress the *ortho*-to-*para* conversion by a factor of six, do not significantly impact the final distribution.

3.4. Line-of-sight Integration Effects

One remaining concern regards the estimation of T_{01} in a diffuse molecular cloud from the column densities of $J = 0$ and $J = 1$, which are integrated quantities along the line of sight. If some of the H_2 resides in hotter, mostly atomic gas where H_3^+ is not abundant, that hot H_2 would cause the observed line of sight T_{01} to exceed T_{01} in the molecular cloud. We expect that such contamination would not be a major effect, as H_2 is known to self-shield very effectively from the interstellar radiation field; thus, the amount of H_2 in primarily atomic (and presumably warmer) gas is likely to be quite small compared to the amount of H_2 in the molecular cloud itself.

To estimate the magnitude of this effect more quantitatively, we take a simple cloud model with a hotter outer region and cooler inner region. Assuming that $T_{01} = 100$ K in the outer region (based on *Copernicus* observations of diffuse atomic clouds; Jenkins et al. 1983), we varied T_{01} in the inner region between 10 K and 100 K for a set of models where the outer region contained 1/2, 1/4, 1/8, and 1/16 of the material in the cloud. We then computed the line of sight T_{01} that would be derived considering both regions of gas. The result of this analysis is shown in Figure 2.

Taking the diffuse cloud model of Neufeld et al. (2005) with a constant density ($n_H = 100$ cm^{-3}) and standard UV radiation field ($\chi_{UV} = 1$) illuminating the cloud from one side, we then determined the amount of H_2 expected to be in the outer region for comparison with observed H_2 column densities in diffuse clouds. We define the transition from the outer to inner regions to be at $E(B-V) = 0.04$ ($N_H \approx 2.3 \times 10^{20}$ cm^{-2}), about half of the total color excess (hydrogen column density) found to supply self-shielding effects in H_2 (Savage et al. 1977; Gillmon & Shull 2006). Integrating $n(H_2)$ in the outer region gives $N_{outer}(H_2) = 6 \times 10^{19}$ cm^{-2}. Because this model effectively only treats one side of a cloud, we compare this value to half of the total H_2 column densities reported in Table 3. The two extreme cases are HD 110432 and HD 154368, where the outer region accounts for about 1/4 and 1/12 of the total cloud, respectively. Taking the observed values of T_{01} and using the appropriate curves on Figure 2, we estimate the temperature of the inner cloud region for each of the five sight lines considered herein. The results are marked in Figure 2 as cross hairs, and show that the line-of-sight values of T_{01} overestimate the inferred inner cloud values of T_{01} by only about 5–10 K. As such, the observed values of T_{01} should be relatively close to the true values of T_{01} in molecular clouds. We therefore assume for the remainder of this paper that the line of sight T_{01} does represent the diffuse molecular cloud kinetic temperature.

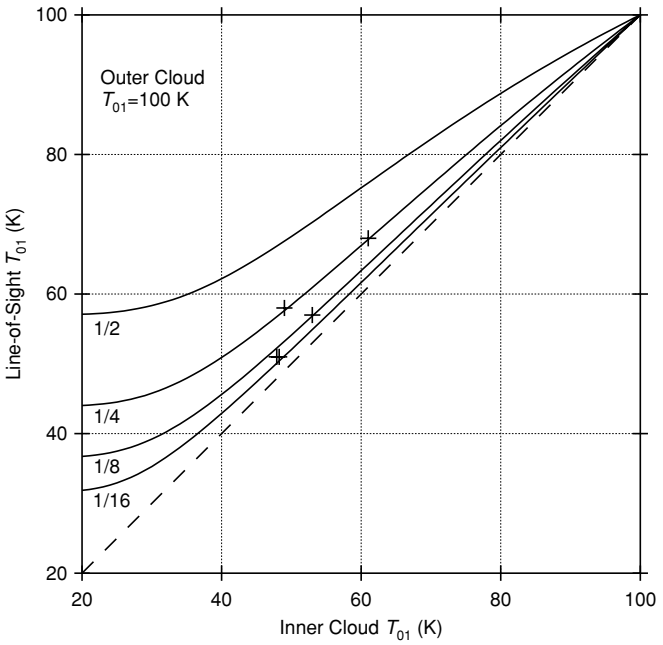

Figure 2. Line-of-sight rotational temperature, T_{01}, is determined for a cloud containing both a warm and cold component. The cold, inner component is varied between 10 K and 100 K, while the warm, outer component is set at 100 K. Different curves show the results for cases where the warm component contains 1/2, 1/4, 1/8, and 1/16 of the total material in the cloud, and are labeled accordingly. Cross hairs mark the inferred inner cloud values of T_{01} given the observed line-of-sight values of T_{01} and estimated fractions of H_2 in a 100 K cloud component for the four sight lines considered herein. From left to right the cross hairs mark HD 73882, HD 154368, ζ Per, X Per, and HD 110432.

3.5. Summary on H_2 Temperature

From the preceding discussions, we conclude that UV measurements accurately measure the column densities of $J = 0$ and $J = 1$ of H_2 in diffuse clouds, that the chemical reaction between H^+ and H_2 occurs $\sim 10^3$ times during the life of an average H_2, and that the steady state of this chemical reaction leads to an *ortho*:*para* ratio that closely reflects the kinetic temperature of the gas. Furthermore, we conclude that it is unlikely that the integration along the line of sight introduces significant contamination of the inferred T_{01}. In summary, then, measured values of T_{01} in diffuse molecular clouds should accurately reflect the cloud kinetic temperature. Consequently, the excitation temperature of H_3^+, which is significantly lower than T_{01}, must not always reflect the kinetic temperature.

4. *ORTHO*- AND *PARA*-H_3^+

Having shown that the temperature discrepancy between T_{01} and $T(H_3^+)$ in diffuse molecular clouds is real and that T_{01} accurately reflects the cloud kinetic temperature, we now consider the processes related to H_3^+ thermalization in diffuse molecular clouds to examine why $T(H_3^+)$ might not match the kinetic temperature.

4.1. Nascent and Thermalized Para-H_3^+ Fractions

H_3^+ is produced by the reaction

$$H_2 + H_2^+ \rightarrow H_3^+ + H, \quad (1)$$

which follows the cosmic-ray ionization of H_2 to form H_2^+. The nuclear spin modification of the product H_3^+ depends on the nuclear spin modifications of the reactant H_2 and H_2^+ according

Table 4
Nascent *Para*-H_3^+ Fraction

Reaction	Collision Fraction	Branching Fraction	p-H_3^+ Fraction
p-H_2^+ + p-H_2	$(p_2)^2$	1	p_2^2
p-H_2^+ + o-H_2	$p_2(1-p_2)$	2/3	$(2/3)(1-p_2)p_2$
o-H_2^+ + p-H_2	$(1-p_2)p_2$	2/3	$(2/3)(1-p_2)p_2$
o-H_2^+ + o-H_2	$(1-p_2)^2$	1/3	$(1/3)(1-p_2)^2$
Total	...	...	$(1/3)+(2/3)p_2$

Notes. This table presents the calculation of the nascent p-H_3^+ fraction formed in diffuse molecular clouds from the $H_2^+ + H_2$ reaction, assuming that cosmic-ray ionization of H_2 to form H_2^+ does not affect its nuclear spin configuration. The collision fraction represents the fraction of total $H_2^+ + H_2$ collisions with the specified nuclear spin configurations. The branching fractions are for p-H_3^+ formation, and are derived from nuclear spin selection rules (Quack 1977; Oka 2004). The final column presents the calculation of the nascent p-H_3^+ fraction.

to the selection rules given by Oka (2004). It is most convenient to express the nuclear spin modifications in terms of the *para*-fractions, rather than the *ortho*:*para* ratios, so we define

$$p_2 \equiv \frac{n(p\text{-}H_2)}{n(p\text{-}H_2)+n(o\text{-}H_2)}$$

and

$$p_3 \equiv \frac{n\left(p\text{-}H_3^+\right)}{n\left(p\text{-}H_3^+\right)+n\left(o\text{-}H_3^+\right)}.$$

As the cosmic-ray ionization of H_2 is not expected to affect the nuclear spin modification, we can further assume that the *para*-fraction of H_2^+ is also given by p_2. Table 4 demonstrates, using these reactant fractions and the nuclear spin branching fractions, that the *para*-fraction of newly formed H_3^+ is $p_3 = (1/3)+(2/3)p_2$, assuming that the rate for the $H_2^+ + H_2$ reaction is independent of nuclear spin configuration.

In diffuse molecular clouds, the vast majority of the H_2 population lies in the lowest *ortho* and *para* states, as the temperature of 70 K is well below the energy of the next states (the $J = 2$ state lies 510 K above $J = 0$, and $J = 3$ lies 844 K above $J = 1$). Therefore, to derive p_2 from astronomical observations, we use the formula $p_2 = N(0)/[N(0)+N(1)]$. H_3^+ on the other hand does have energetically accessible *para* states, as the (2,2) and (2,1) states lie only 151.3 and 249.2 K above the (1,1) ground state. However, the (2,2) and (2,1) states are expected to quickly undergo radiative decay to the (1,1) state at the temperatures and densities of the diffuse molecular clouds (Oka & Epp 2004). Furthermore, population in the next *ortho* state (3,3) has not been observed in these environments (Oka et al. 2005), so the vast majority of o-H_3^+ is in the (1,0) state. Consequently, to calculate p_3 from the astronomical observations, we use $p_3 = N(1,1)/[N(1,1)+N(1,0)]$.

Figure 3 shows the nascent p_3 distribution as a function of p_2. This figure also shows the total *para*-fraction of a thermalized sample of H_3^+ at various temperatures, calculated using the energy levels $E(J, K)$ from Lindsay & McCall (2001). Also plotted in the figure are the results of the astronomical observations presented in Table 3. In diffuse molecular clouds, p_3 generally appears to lie between the nascent p_3 and the thermal p_3 values, suggesting an incomplete thermalization of the nuclear spin modifications of H_3^+.

As discussed by Oka & Epp (2004), the aforementioned spontaneous emission from the (2,2) and (2,1) states decreases $T(H_3^+)$ relative to T_{01}. They show that for a cloud density of 100 cm^{-3} and $60 \leqslant T_{01} \leqslant 120$ K, $T(H_3^+)$ should fall in the

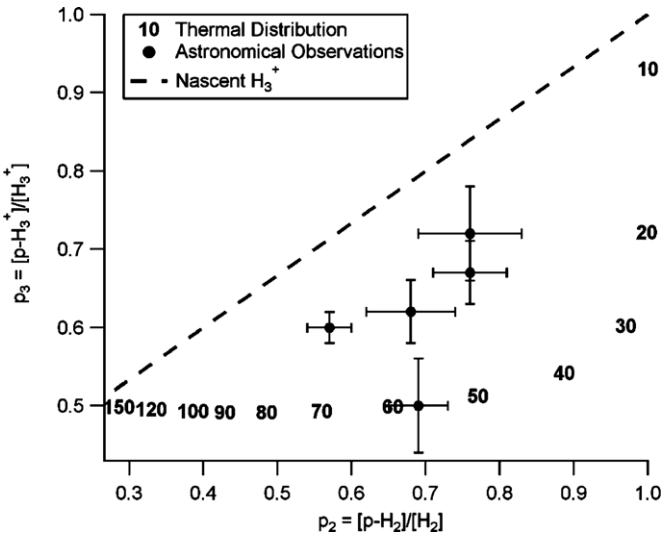

Figure 3. Nascent (dashed line) and thermalized (numbers, in K) p-H_3^+ fraction as a function of the p-H_2 fraction. The circles represent the observations of diffuse molecular clouds summarized in Table 3 with 1σ uncertainties.

range of 40–50 K, and this accounts for a ~40–80 K difference between T_{01} and $T(H_3^+)$. However, in the temperature ranges discussed here, the *para*-fractions of H_3^+ and H_2 are nonlinear with respect to these excitation temperatures. In terms of p_3, all $T(H_3^+)$ above about 40 K should have about the same p_3, while p_3 changes substantially when $T(H_3^+)$ falls below 40 K, as can be seen in Figure 3. Spontaneous emission will raise the apparent p_3 (as derived from the N(1,1):N(1,0) ratio) relative to the thermalized p_3 and consequently lower $T(H_3^+)$ with respect to T_{01}. However, Figure 3 illustrates that the magnitude of this effect cannot account for the discrepancy observed in the astronomical observations in these environments in terms of the *para*-fractions, with the possible exception of X Per.

4.2. The Reaction of H_3^+ with H_2

As in the case of H_2, the nuclear spin modifications of H_3^+ cannot effectively be changed by radiative transitions or by non-reactive collisions; only chemical reactions can do so. In this case, the reaction $H_3^+ + H_2 \rightarrow (H_5^+)^* \rightarrow H_2 + H_3^+$ is the most efficient mechanism for interconverting o-H_3^+ and p-H_3^+. When H_3^+ and H_2 collide, there are three possible reaction outcomes:

$$\tilde{H}_3^+ + H_2 \rightarrow \tilde{H}_3^+ + H_2 \text{ (identity)}, \quad (2)$$

$$\tilde{H}_3^+ + H_2 \rightarrow H_2\tilde{H}^+ + \tilde{H}_2 \text{ (hop), and} \quad (3)$$

$$\tilde{H}_3^+ + H_2 \rightarrow H\tilde{H}_2^+ + H\tilde{H} \text{ (exchange).} \quad (4)$$

In the case of Reaction (2), the nuclear spin configurations of the H_3^+ and H_2 remain unchanged, while in Reactions (3) and (4) the configuration may change. However, like Reaction (1), the hop and exchange pathways must obey nuclear spin selection rules (Quack 1977; Oka 2004). For instance, in order for a reaction between p-H_3^+ and p-H_2 to form o-H_3^+ the reaction must be an exchange, and o-H_2 must also be formed to conserve the total nuclear spin angular momentum.

A potential energy surface based on high-level ab initio calculations is available for the H_5^+ system (Xie et al. 2005). Based on the surface stationary points, a barrier of 52.2 cm^{-1} must be overcome for a hop Reaction (3) to occur, and a

barrier of 1565.9 cm^{-1} for an exchange Reaction (4) to occur. The dissociation energy D_e is calculated to be 2903 cm^{-1}; therefore, $(H_5^+)^*$ formed from association of H_3^+ with H_2 has sufficient energy to overcome these barriers. As such, the complex may undergo many hop and exchange processes over its lifetime, and given sufficient time, the product distribution may approach a statistical limit. As the statistical weights for the hop and exchange reactions are 3 and 6, respectively, the branching ratio $\alpha \equiv k_3/k_4$ is 0.5 in the statistical limit. Quantum reactive scattering calculations are presently unavailable on this potential energy surface, so experimental data are necessary for determining the value of α, as well as its temperature dependence.

The only experimental determination of α for the $H_3^+ + H_2$ system was performed by Cordonnier et al. (2000). This study was done by spectroscopically measuring the *ortho*-to-*para* ratio of H_3^+ formed in a discharge of pure *p*-H_2 at 400 K, and under these conditions, the value $\alpha = 2.4$ was derived. No measurements at lower temperatures have been reported for this system, but the isotopically substituted reaction $D_3^+ + H_2$ has been studied at a variety of collision energies using an ion trap/guided beam technique (Gerlich 1993). It was observed that α varies substantially with the D_3^+–H_2 collision energy. As this energy decreases, α approaches the statistical value of 0.5, and the value 2.4 is reached at an energy corresponding to the average collision energy at ∼440 K, in general agreement with the study by Cordonnier et al. (2000). However, a direct comparison of these results to H_3^+ in the interstellar medium is problematic owing to the endothermicity of the reaction channel and the non-thermal reactant internal state distribution in the experimental measurement.

The final consideration for this reaction is the fraction of reactions that lead to no change in the nuclear spin modification, S^{id}. A large value for S^{id} would indicate that nuclear-spin-changing collisions are a small fraction of the total number of $H_3^+ + H_2$ collisions, and the thermalization process would be slower than the collision rate. In fact, there is experimental evidence for this, as studies of the $H_3^+ + HD \rightarrow H_2D^+ + H_2$ reaction give a rate coefficient of 3.5×10^{-10} cm^3 s^{-1} (Gerlich et al. 2002), much slower than the Langevin rate coefficient 1.7×10^{-9} cm^3 s^{-1}. These results lead to $S^{id} \sim 0.8$, but it is possible that S^{id} could be different for the purely hydrogenic system, which is thermoneutral rather than exothermic.

4.3. Steady-state Para-H_3^+ Fraction from $H_3^+ + H_2$: "Bimolecular Reactive Equilibrium"

After taking into account its chemical physics, does the steady state of the $H_3^+ + H_2$ chemical reaction lead to a completely thermalized p_3 in the interstellar medium? To consider this question, we have constructed a simple steady-state model for *ortho*- and *para*-H_3^+, in terms of nuclear-spin-dependent rate coefficients k_{xxxx} for each potential sub-reaction (e.g., k_{oppo}: *o*-$H_3^+ + p$-$H_2 \rightarrow p$-$H_3^+ + o$-H_2). The derivation of this model, which we shall call the "bimolecular reactive equilibrium" (BRE) model, is presented in Appendix B, and the resulting expression for p_3 is given in the Appendix as Equation (B4).

The rate coefficients themselves were computed using the prescription of Park & Light (2007), which takes into account both the nuclear spin branching fractions as well as energetic considerations at the state-to-state level, using a microcanonical approach. This work has since been extended by Hugo et al. (2009) to deuterated versions of this chemical reaction, and the latter authors report quantitative agreement between the two sets of calculations. We therefore judge these rate coefficients to be reliable within the context of this theoretical approach.

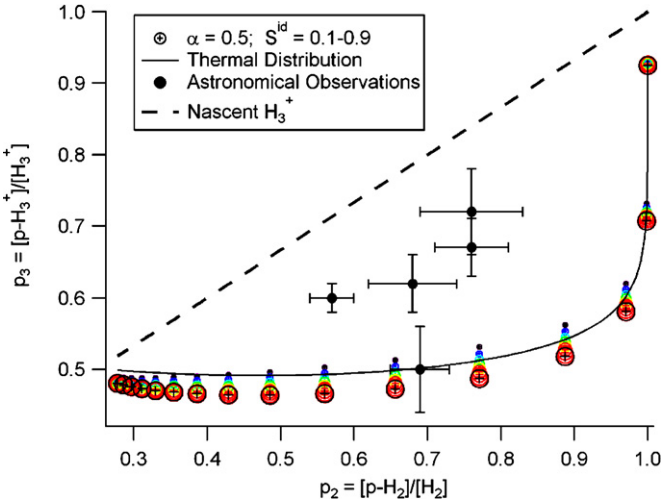

Figure 4. BRE calculations of the *para*-H_3^+ fraction as a function of the *para*-H_2 fraction, under the influence of the $H_3^+ + H_2$ reaction. The thin solid line represents the thermal limit (as in Figure 3), and the circled crosses represent the results of our calculations (based on Park & Light's model) for $\alpha = 0.5$ and various values of S^{id} ranging from 0.1 (small purple) to 0.9 (large brown). Each cluster of crosses represents a calculation at a single temperature, ranging from 10 K (upper right) to 160 K (lower left) in steps of 10 K. Also plotted are the nascent H_3^+ distribution and the astronomical observations.

(A color version of this figure is available in the online journal.)

The Park & Light code (provided by K. Park 2009, private communication) requires five input parameters: the kinetic temperature, the rotational temperature of H_3^+ and H_2, and the three branching fractions S^{id}, S^{hop}, and S^{exch}. For these calculations, the rotational temperature was held at 10 K in each nuclear spin manifold in order to have the vast majority of *o*-H_3^+ in (1,0) and *p*-H_3^+ in (1,1). Therefore, we express the inputs to the model in terms of only three parameters: $T \equiv T_{kin}$, S^{id}, and α, as $S^{id} + S^{hop} + S^{exch} = 1$ and $\alpha = S^{hop}/S^{exch}$. The code then outputs all of the rate coefficients required in Equation (B4). For a single set of branching fraction values, the rate coefficients were calculated for $10 \leqslant T \leqslant 160$ K in steps of 10 K, and p_2 was set to its thermal value for each calculation.

Figure 4 shows the results of the BRE model for a fixed value of $\alpha = 0.5$ for various values of S^{id} ranging from 0.1 to 0.9; similarly, Figure 5 shows results for fixed $S^{id} = 0.5$ and various α ranging from 0 to ∞. The results of the calculation are not particularly sensitive to the fraction of collisions that are reactive (as traced by S^{id}) or the ratio of the hop to exchange outcomes (α). Since in all cases p_3 falls near its thermal value, these results suggest that regardless of the values of α or S^{id}, the $H_3^+ + H_2$ reaction should essentially thermalize the H_3^+ nuclear spin species. This stands in clear contradiction to the reported astronomical observations in diffuse molecular clouds, with the exception of X Per. The discrepancy between T_{01} and $T(H_3^+)$ cannot be explained by the BRE model, and must then be explained by a lack of equilibration via this chemical reaction.

An interesting aspect of these results is that the steady state p_3 at some temperatures is actually *below* the value of 0.5 expected based on statistical weights alone (often called the

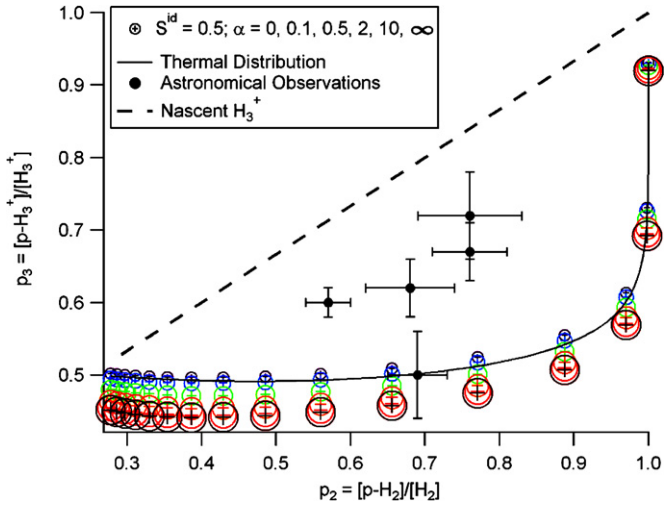

Figure 5. Same as Figure 4, except that S^{id} is held at 0.5 and α varies between 0 (small purple) and ∞ (large brown).

(A color version of this figure is available in the online journal.)

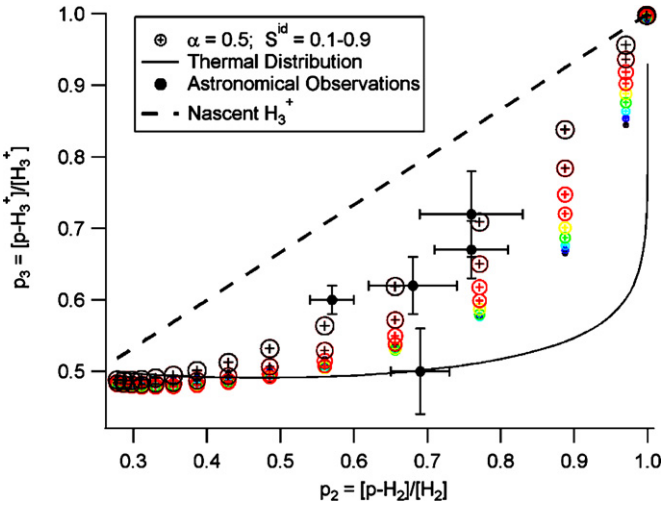

Figure 6. Steady-state calculations of the *para*-H_3^+ fraction as a function of the *para*-H_2 fraction, under the influence of both the $H_3^+ + H_2$ reaction and dissociative recombination. The plotted quantities are analogous to those in Figure 4. In this case, the *o*-H_3^+ and *p*-H_3^+ DR rate coefficients $k_{e,o}$ and $k_{e,p}$ are assumed to be equal and taken from McCall et al. (2004). Each vertical cluster of points represents a calculation at a single temperature, beginning at 160 K in the lower left and decreasing by 10 K each point moving to the right.

(A color version of this figure is available in the online journal.)

"high-temperature limit"). This appears to be a robust result for $\alpha > 0.5$, at least in the range of S^{id} explored here. This effect may have been observed experimentally in our group's recent measurements of supersonically expanding hydrogen plasmas. Tom et al. (2010) reported $p_3 = 0.491 \pm 0.024$ for a normal hydrogen ($p_2 = 0.25$) plasma at $\sim$ 80 K, and Kreckel et al. (2010) reported $p_3 = 0.479 \pm 0.02$ in a warmer ($\sim$200 K) normal hydrogen and argon plasma.[9] Finally, in work outside our laboratory, Kreckel et al. (2007) have reported $p_3 = 0.4$ in a low-temperature ion trap. All of these measurements suggest that it is in fact possible to achieve $p_3 < 0.5$, and lend some evidence to support the calculated results.

4.4. Steady-state Para-H_3^+ Fraction from $H_3^+ + H_2$ and $H_3^+ + e^-$

We now consider whether there are enough reactive collisions within the lifetime of an average H_3^+ in diffuse molecular clouds to bring the spin modifications into BRE. The destruction of H_3^+ in such clouds is dominated by dissociative recombination (DR) with electrons, and the lifetime is simply $\tau_{\rm life} = (k_{\rm DR} n(e^-))^{-1}$ (the reciprocal of the destruction rate), where $k_{\rm DR}$ is the DR rate coefficient. The average time between reactive collisions can be expressed as $\tau_{\rm rxn} = (k_{\rm rc} n({\rm H_2}))^{-1}$, where $k_{\rm rc}$ is the reactive collision rate for $H_3^+ + H_2$. The average number of collisions an H_3^+ will experience is then $\mathcal{N}_{\rm rxn} = \tau_{\rm life}/\tau_{\rm rxn} = [k_{\rm rc}/k_{\rm DR}][n({\rm H_2})/n(e^-)]$.

Assuming for the moment that $k_{\rm DR}$ is independent of the nuclear spin modification, we adopt a typical value (for $T \sim 70$ K) of $k_{\rm DR} = 2 \times 10^{-7}$ cm^3 s^{-1} (McCall et al. 2004). The ratio $n({\rm H_2})/n(e^-)$ can be rewritten as $f/2x_e$, where x_e is the electron fraction, typically 1.5×10^{-4} assuming charge neutrality and that C^+ is the dominant ionic species (Cardelli et al. 1996; Sofia et al. 2004). If we adopt $f = 0.9$, and take $k_{\rm rc}$ to be the full collision rate of $H_3^+ + H_2$ (1.9×10^{-9} cm^3 s^{-1}; Park 2007), we find that $\mathcal{N}_{\rm rxn} \sim 20$. However, if we instead adopt the smaller reactive rate coefficient $\sim 3 \times 10^{-10}$ cm^3 s^{-1} of Gerlich et al. (2002), we find that $\mathcal{N}_{\rm rxn} \sim 5$. With such a small number of collisions in the lifetime of H_3^+, p_3 may not reach the value predicted by Equation (B4). In Appendix C, we derive a more complete steady-state expression (Equation (C7)) including the effects of both the $H_3^+ + H_2$ reaction and nuclear-spin-dependent DR rates ($k_{e,p}$ and $k_{e,o}$ for *p*-H_3^+ and *o*-H_3^+).

We call this model simply the "steady-state" model, and we adopt the values $f = 0.9$ and $x_e = 1.5 \times 10^{-4}$ as before. Figure 6 shows the results of this steady-state model if we assume that the DR rate coefficient is the same for both nuclear spin modifications. (We have adopted the temperature-dependent value of McCall et al. 2004.) In this case, the values of p_3 depend quite sensitively on S^{id}, as this represents the fraction of $H_3^+ + H_2$ collisions that are nonreactive during the relatively short lifetime of H_3^+. Consequently with higher values of S^{id} (larger circles in Figure 6), the *p*-H_3^+ fraction in the steady state is closer to the nascent fraction. For $S^{id} = 0.9$, which corresponds to a reactive rate coefficient of $k_{\rm rc} = 1.9 \times 10^{-10}$ cm^3 s^{-1}, the calculated p_3 are in reasonable agreement with most of the observations. The upper range of the X Per uncertainty is consistent with $S^{id} = 0.7$.

In Figure 7, we instead consider the calculated DR rate coefficients for *ortho*- and *para*-H_3^+ presented in dos Santos et al. (2007). Their prediction is that *p*-H_3^+ is destroyed considerably faster by electrons at low temperatures than *o*-H_3^+; consequently, even for large values of S^{id}, the steady-state p_3 does not approach either the nascent or astronomically observed values. In the absence of the $H_3^+ + H_2$ reaction ($S^{id} = 1$), p_3 would be governed by a steady state determined by the competition between the formation and the spin-dependent DR processes, and this is shown in Figure 8.

If the calculated rate coefficients of dos Santos et al. (2007) are correct, it is difficult to explain the observed p_3. This is because, with the exception of X Per, the observed p_3 are higher than the curve resulting from the steady state of H_3^+ formation and destruction using these DR rate coefficients, and inclusion of the $H_3^+ + H_2$ reaction further drives p_3 toward the

[9] Recent measurements in our laboratory have confirmed, with higher statistical significance, $p_3 < 0.5$ in hollow cathode plasmas containing normal hydrogen. These results will be reported elsewhere, but it should be noted that p_3 in these plasmas may be influenced by three-body collisions due to the higher number densities.

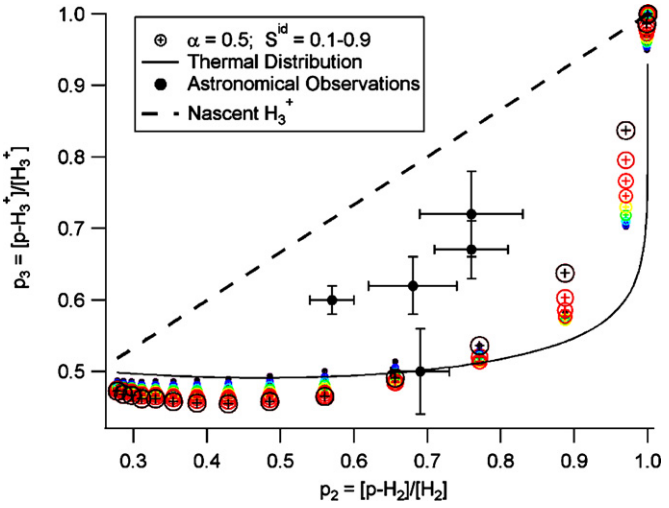

Figure 7. Same as Figure 6, except using the spin-dependent DR rate coefficients from dos Santos et al. (2007).

(A color version of this figure is available in the online journal.)

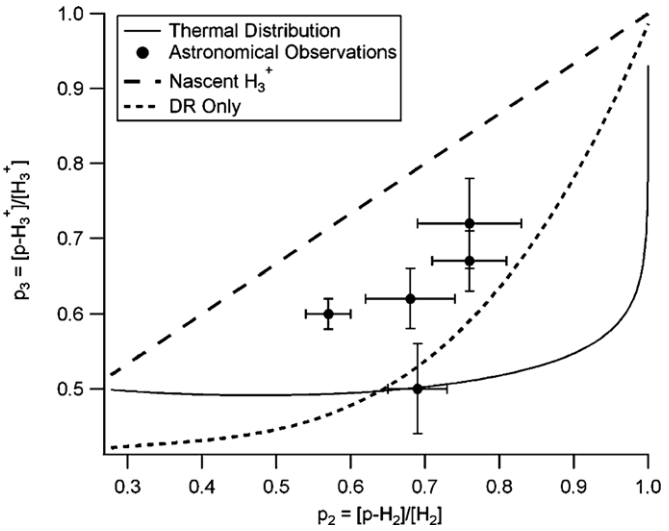

Figure 8. Steady-state calculations of the *para*-H_3^+ fraction as a function of the *para*-H_2 fraction, under the influence of formation and DR only. The solid line shows the thermal limit, and the dotted line represents the results of our calculations, where we have used the spin-dependent DR rate coefficients from dos Santos et al. (2007). Also plotted are the nascent H_3^+ distribution (dashed line) and the astronomical observations.

value expected for thermal equilibrium. Recent storage ring experiments by Tom et al. (2009) and Kreckel et al. (2005) both saw an increased DR cross section when H_3^+ is produced from *p*-H_2; however, recent imaging results presented in Kreckel et al. (2010) suggest that the ions in these experiments have been heated during extraction from the ion sources, and the difference between the *o*-H_3^+ and *p*-H_3^+ may therefore have been overestimated. Further experimental work is clearly needed to pin down the enhancement (if any) in *p*-H_3^+ DR, and confirmation of the theoretical predictions would also be quite helpful.

To summarize, according to our models the reaction of H_3^+ with H_2 is expected to effectively thermalize the nuclear spin configurations of H_3^+ at steady state, provided that sufficient collisions occur within the lifetime of an H_3^+. In diffuse molecular clouds, however, the average number of reactive collisions with H_2 suffered by an H_3^+ is small, indicating that the formation and destruction rates of the two nuclear spin species should be important. A more complete model which takes these factors into account reaches reasonable agreement with observations in four of five sight lines provided S^{id} is on the order of 0.9 and *o*-H_3^+ and *p*-H_3^+ are destroyed at equal rates owing to DR. Reconciling the observations with the spin-dependent theoretical rates of dos Santos et al. (2007) is difficult, and accurate experimental measurements of the spin-dependent DR rates of H_3^+ at low temperature are needed.

5. CONCLUSIONS

While all evidence seems to suggest that T_{01} inferred from ultraviolet spectroscopy of H_2 accurately reflects the kinetic temperature of diffuse molecular clouds, the observed excitation temperature of H_3^+ is clearly non-thermal in four of the five measured sight lines. Based on the microcanonical model of Park & Light (2007), we have constructed a steady-state model to predict the *para*-H_3^+ fraction (p_3) if reactive collisions between H_3^+ and H_2 control the spin modifications of H_3^+. Those results show p_3 close to the limit expected for full thermalization, and far from the observations. However, a steady-state model that incorporates both the $H_3^+ + H_2$ reaction as well as the H_3^+ formation (following cosmic-ray ionization) and destruction (by electron recombination) can reproduce the observed p_3 if the reactive collision rate is somewhat slow and the DR rates for *ortho*- and *para*-H_3^+ are comparable. Our interpretation, given the currently available data, is that H_3^+ suffers relatively few spin-changing collisions with H_2 in its lifetime, and is thus incompletely equilibrated by this reaction. The observed *para*-H_3^+ fraction therefore lies between the nascent fraction and the nearly thermal fraction that would be reached with sufficient reactive collisions. If our model is correct (and the spin-dependent DR rates of H_3^+ are nearly equal at low temperature), this marks the first determination of the reactive rate coefficient of the $H_3^+ + H_2$ reaction, and suggests a value on the order of 10^{-10} cm^{-3} s^{-1}.

Fully quantum reactive scattering calculations of the $H_3^+ + H_2$ reaction would be highly desirable, as they would pin down the state-to-state rate coefficients needed to predict the interstellar *para*-H_3^+ fraction. Further experiments and theoretical calculations to elucidate the dependence (if any) of the DR on the nuclear spin modification of H_3^+ are also urgently needed. Once the effects of the reactive collisions and DR are fully understood, the *para*-H_3^+ fraction in diffuse molecular clouds can be calculated as a function of the kinetic temperature and the ratio of the molecular fraction to the electron fraction. This, in turn, suggests that H_3^+ may become a useful "thermometer" for diffuse molecular clouds with high extinction, where ultraviolet measurements of H_2 are not feasible. However, the calibration of this thermometer will require further experimental and theoretical efforts.

The authors thank Brian L. Rachford for helpful discussions about the T_{01} determinations, Takeshi Oka for helpful conversations about *ortho*- and *para*-H_3^+, Kisam Park for providing the code to determine the nuclear-spin-dependent rate coefficients for the $H_3^+ + H_2$ reaction, and the anonymous referee for helpful comments. This work has been supported by NSF grant PHY08-55633. This work is based in part on observations obtained at the Gemini Observatory, which is operated by the Association of Universities for Research in Astronomy, Inc., under a cooperative agreement with the NSF on behalf of the Gemini partnership: the National Science Foundation

Table 5
Reactions and Rate Equations Used in Models

Number	Reaction	Rate	Comments
1	$H_2 + CR \rightarrow H_2^+ + e^- + CR'$	$\zeta_2[H_2]$	Cosmic-ray ionization
2	$H_2 + H_2^+ \rightarrow H_3^+ + H$	$k_1[H_2][H_2^+]$	H_3^+ formation (see Table 1)
3	i-$H_3^+ + j$-$H_2 \rightarrow m$-$H_3^+ + n$-H_2	$k_{ijmn}[i$-$H_3^+][j$-$H_2]$	Thermalization reaction for H_3^+
4	p-$H_3^+ + e^- \rightarrow H_2 + H$ (or) 3H	$k_{e,p}[p$-$H_3^+][e^-]$	p-H_3^+ DR
5	o-$H_3^+ + e^- \rightarrow H_2 + H$ (or) 3H	$k_{e,o}[o$-$H_3^+][e^-]$	o-H_3^+ DR

Notes. The branching fractions for o-H_3^+ and p-H_3^+ in Reaction (2) are assumed to be given by nuclear spin statistics. In Reaction (3), i, j, m, and n represent the nuclear spin configurations of the respective species (o or p). Some of these 16 reactions are forbidden by nuclear spin selection rules, and others are not used directly in the derivation because they do not result in a change in the H_3^+ nuclear spin configuration. The square brackets refer to the number density of the species.

(United States), the Science and Technology Facilities Council (United Kingdom), the National Research Council (Canada), CONICYT (Chile), the Australian Research Council (Australia), Ministério da Ciência e Tecnologia (Brazil) and Ministerio de Ciencia, Tecnología e Innovación Productiva (Argentina). Gemini/Phoenix spectra were obtained through programs GS-2009B-Q-71 and GS-2010A-Q-60. This paper is also based in part on observations obtained with the Phoenix infrared spectrograph, developed and operated by the National Optical Astronomy Observatory.

APPENDIX A

REACTIONS AND RATES

In this appendix, we derive the formulas for the BRE and steady-state *para*-H_3^+ fractions. We consider four processes: cosmic-ray ionization of H_2, formation of H_3^+, the $H_3^+ + H_2$ reaction, and DR of H_3^+. If all nuclear spin configurations are considered, this gives a total of 28 reactions. The chemical reactions used in the model and their rate expressions are summarized in Table 5. It should be noted that for this section, we employ the chemist's notation of using the square brackets to refer to the number density of the respective species.

APPENDIX B

DERIVATION: BIMOLECULAR REACTIVE EQUILIBRIUM MODEL

Consider the case that H_3^+ formation and destruction are slow compared with the $H_3^+ + H_2$ reaction. We can then ignore formation and destruction processes and write the rate equation for p-H_3^+ only in terms of the latter reaction:

$$\frac{d}{dt}[p\text{-}H_3^+] = \{(k_{oopo} + k_{oopp})[o\text{-}H_2] + (k_{oppo} + k_{oppp})[p\text{-}H_2]\}[o\text{-}H_3^+] - \{(k_{pooo} + k_{poop})[o\text{-}H_2] + (k_{ppoo} + k_{ppop})[p\text{-}H_2]\}[p\text{-}H_3^+]. \quad \text{(B1)}$$

Assuming the steady state, Equation (B1) is equal to 0. The right side can then be divided by $[H_3^+][H_2]$ in order to express the rate in terms of p_2 and p_3 as follows:

$$0 = \{(k_{oopo} + k_{oopp})(1 - p_2) + (k_{oppo} + k_{oppp})p_2\}(1 - p_3) - \{(k_{pooo} + k_{poop})(1 - p_2) + (k_{ppoo} + k_{ppop})p_2\}p_3. \quad \text{(B2)}$$

The resultant equation can be solved for p_3:

$$p_3 = \frac{(k_{oopp} + k_{oopo})(1 - p_2) + (k_{oppo} + k_{oppp})p_2}{(k_{oopp} + k_{oopo} + k_{poop} + k_{pooo})(1 - p_2) + (k_{oppo} + k_{oppp} + k_{ppoo} + k_{ppop})p_2}. \quad \text{(B3)}$$

Owing to nuclear spin selection rules, the rate coefficients k_{oppp} and k_{ppop} are rigorously 0. Removal of these terms gives the final result:

$$p_3 = \frac{(k_{oopp} + k_{oopo})(1 - p_2) + k_{oppo}p_2}{(k_{oopp} + k_{oopo} + k_{poop} + k_{pooo})(1 - p_2) + (k_{oppo} + k_{ppoo})p_2}. \quad \text{(B4)}$$

APPENDIX C

DERIVATION: STEADY-STATE MODEL

Consider now the case in which H_3^+ formation and DR compete effectively with the $H_3^+ + H_2$ thermalization reaction. We make the assumption that formation of p-H_3^+ from $H_2^+ + H_2$ is governed only by the nuclear spin branching fractions presented in Table 4. Under these conditions, the full rate equation for p-H_3^+ is

$$\frac{d}{dt}[p\text{-}H_3^+] = k_1([p\text{-}H_2][p\text{-}H_2^+] + \frac{2}{3}[p\text{-}H_2][o\text{-}H_2^+] + \frac{2}{3}[o\text{-}H_2][p\text{-}H_2^+] + \frac{1}{3}[o\text{-}H_2][o\text{-}H_2^+])$$
$$+ \{(k_{oopo} + k_{oopp})[o\text{-}H_2] + (k_{oppo} + k_{oppp})[p\text{-}H_2]\}[o\text{-}H_3^+]$$
$$- \{(k_{pooo} + k_{poop})[o\text{-}H_2] + (k_{ppoo} + k_{ppop})[p\text{-}H_2]\}[p\text{-}H_3^+]$$
$$- k_{e,p}[e^-][p\text{-}H_3^+]. \quad \text{(C1)}$$

From Table 4, we can reduce the first line in this equation to $k_1[H_2][H_2^+]\{(1/3) + (2/3)p_2\}$. We now invoke steady-state arguments for all species. For H_2^+, $\zeta_2[H_2] = k_1[H_2][H_2^+]$; therefore, $k_1[H_2^+]$ can be replaced by ζ_2. Setting the resultant equation equal to zero and dividing by $[H_3^+][H_2]$ as before gives

$$0 = \frac{\zeta_2}{[H_3^+]}\left(\frac{1}{3} + \frac{2}{3}p_2\right)$$
$$+ \{(k_{oopo} + k_{oopp})(1 - p_2) + (k_{oppo} + k_{oppp})p_2\}(1 - p_3)$$
$$- \{(k_{pooo} + k_{poop})(1 - p_2) + (k_{ppoo} + k_{ppop})p_2\}p_3$$
$$- k_{e,p}\frac{[e^-]}{[H_2]}p_3. \quad \text{(C2)}$$

This equation can be further simplified by examining the steady-state value of $[H_3^+]$, which begins with the equation $\zeta_2[H_2] = k_e[H_3^+][e^-]$. More specifically, if we include the possibility for different DR rates for $o\text{-}H_3^+$ and $p\text{-}H_3^+$, we obtain the equation

$$\zeta_2[H_2] = [e^-](k_{e,p}[p\text{-}H_3^+] + k_{e,o}[o\text{-}H_3^+]). \quad \text{(C3)}$$

Dividing both sides of Equation (C3) by $[H_3^+][H_2]$ results in an expression for $\zeta_2/[H_3^+]$:

$$\frac{\zeta_2}{[H_3^+]} = \frac{[e^-]}{[H_2]}(k_{e,p}p_3 + k_{e,o}(1 - p_3)). \quad \text{(C4)}$$

Substituting this relation into Equation (C2) gives

$$0 = \frac{[e^-]}{[H_2]}(k_{e,p}p_3 + k_{e,o}(1 - p_3))\left(\frac{1}{3} + \frac{2}{3}p_2\right)$$
$$+ \{(k_{oopo} + k_{oopp})(1 - p_2) + (k_{oppo} + k_{oppp})p_2\}(1 - p_3)$$
$$- \{(k_{pooo} + k_{poop})(1 - p_2) + (k_{ppoo} + k_{ppop})p_2\}p_3$$
$$- k_{e,p}\frac{[e^-]}{[H_2]}p_3. \quad \text{(C5)}$$

Solving for p_3 and removing the k_{oppp} and k_{ppop} terms yield

$$p_3 = \frac{k_{e,o}\frac{[e^-]}{[H_2]}\left(\frac{1}{3} + \frac{2}{3}p_2\right) + (k_{oopp} + k_{oopo})(1 - p_2) + k_{oppo}p_2}{k_{e,p}\frac{[e^-]}{[H_2]}\left(\frac{2}{3} - \frac{2}{3}p_2\right) + k_{e,o}\frac{[e^-]}{[H_2]}\left(\frac{1}{3} + \frac{2}{3}p_2\right) + (k_{oopp} + k_{oopo} + k_{poop} + k_{pooo})(1 - p_2) + (k_{oppo} + k_{ppoo})p_2}. \quad \text{(C6)}$$

Finally, the ratio $[e^-]/[H_2]$ can be replaced by $2x_e/f$, which results in Equation (C7):

$$p_3 = \frac{k_{e,o}\frac{2x_e}{f}\left(\frac{1}{3} + \frac{2}{3}p_2\right) + (k_{oopp} + k_{oopo})(1 - p_2) + k_{oppo}p_2}{k_{e,p}\frac{2x_e}{f}\left(\frac{2}{3} - \frac{2}{3}p_2\right) + k_{e,o}\frac{2x_e}{f}\left(\frac{1}{3} + \frac{2}{3}p_2\right) + (k_{oopp} + k_{oopo} + k_{poop} + k_{pooo})(1 - p_2) + (k_{oppo} + k_{ppoo})p_2}. \quad \text{(C7)}$$

REFERENCES

Cardelli, J. A., Meyer, D. M., Jura, M., & Savage, B. D. 1996, ApJ, 467, 334
Cartledge, S. I. B., Lauroesch, J. T., Meyer, D. M., & Sofia, U. J. 2004, ApJ, 613, 1037
Cordonnier, M., Uy, D., Dickson, R. M., Kerr, K. E., Zhang, Y., & Oka, T. 2000, J. Chem. Phys., 113, 3181
Crawford, I. A. 1995, MNRAS, 277, 458
Dalgarno, A., Black, J. H., & Weisheit, J. C. 1973, Astrophys. Lett., 14, 77
dos Santos, S. F., Kokoouline, V., & Greene, C. H. 2007, J. Chem. Phys., 127, 124309
Gerlich, D. 1990, J. Chem. Phys., 92, 2377
Gerlich, D. 1993, J. Chem. Soc. Faraday Trans., 89, 2199
Gerlich, D., Herbst, E., & Roueff, E. 2002, Planet. Space Sci., 50, 1275
Gibb, E. L., Brittain, S. D., Rettig, T. W., Troutman, M., Simon, T., & Kulesa, C. 2010, ApJ, 715, 757
Gillmon, K., & Shull, J. M. 2006, ApJ, 636, 908
Glassgold, A. E., & Langer, W. D. 1974, ApJ, 193, 73
Goto, M., McCall, B. J., Geballe, T. R., Usuda, T., Kobayashi, N., Terada, H., & Oka, T. 2002, PASJ, 54, 951
Gry, C., Boulanger, F., Nehmé, C., Pineau des Forêts, G., Habart, E., & Falgarone, E. 2002, A&A, 391, 675
Hinkle, K. H., et al. 2003, Proc. SPIE, 4834, 353
Hugo, E., Asvany, O., & Schlemmer, S. 2009, J. Chem. Phys., 130, 164302
Indriolo, N., Geballe, T. R., Oka, T., & McCall, B. J. 2007, ApJ, 671, 1736
Jenkins, E. B., Jura, M., & Loewenstein, M. 1983, ApJ, 270, 88
Jensen, A. G., Rachford, B. L., & Snow, T. P. 2005, ApJ, 619, 891
Käufl, H., et al. 2004, Proc. SPIE, 5492, 1218
Kreckel, H., et al. 2005, Phys. Rev. Lett., 95, 263201
Kreckel, H., et al. 2007, J. Phys.: Conf. Ser., 88, 012064
Kreckel, H., et al. 2010, Phys. Rev. A, 82, 042715
Lindsay, C. M., & McCall, B. J. 2001, J. Mol. Spectrosc., 210, 60
McCall, B. J., Geballe, T. R., Hinkle, K. H., & Oka, T. 1998a, Science, 279, 1910
McCall, B. J., Hinkle, K. H., Geballe, T. R., & Oka, T. 1998b, Faraday Discuss., 109, 267
McCall, B. J., et al. 2003, Nature, 422, 500
McCall, B. J., et al. 2004, Phys. Rev. A., 70, 052716
Neufeld, D. A., Wolfire, M. G., & Schilke, P. 2005, ApJ, 628, 260
Oka, T. 2004, J. Mol. Spectrosc., 228, 635
Oka, T., & Epp, E. 2004, ApJ, 613, 349
Oka, T., Geballe, T. R., Goto, M., Usuda, T., & McCall, B. J. 2005, ApJ, 632, 882
Park, K., & Light, J. C. 2007, J. Chem. Phys., 126, 044305
Quack, M. 1977, Mol. Phys., 34, 477
Rachford, B. L., et al. 2002, ApJ, 577, 221
Rachford, B. L., et al. 2009, ApJS, 180, 125
Savage, B. D., Bohlin, R. C., Drake, J. F., & Budich, W. 1977, ApJ, 216, 291
Snow, T. P., & McCall, B. J. 2006, ARA&A, 44, 367
Sofia, U. J., Lauroesch, J. T., Meyer, D. M., & Cartledge, S. I. B. 2004, ApJ, 605, 272
Spitzer, L., Jr. 1978, Physical Processes in the Interstellar Medium (New York: Wiley-Interscience)
Takahashi, J. 2001, ApJ, 561, 254
Tom, B. A., Mills, A. A., Wiczer, M. B., Crabtree, K. N., & McCall, B. J. 2010, J. Chem. Phys., 132, 081103
Tom, B. A., et al. 2009, J. Chem. Phys., 130, 031101
Woodall, J., Agúndez, M., Markwick-Kemper, A. J., & Millar, T. J. 2007, A&A, 466, 1197
Xie, Z., Braams, B. J., & Bowman, J. M. 2005, J. Chem. Phys., 122, 224307